https://doi.org/10.5194/esurf-2021-77
Preprint. Discussion started: 10 November 2021

Earth Surface Dynamics Discussions
Open Access
EGU

Entrainment and deposition of boulders in a gravel bed river

Pascal Allemand[1], Eric Lajeunesse[2], Olivier Devauchelle[2], Vincent Langlois[1]

[1]Université Claude Bernard Lyon 1, ENS Lyon, Université Jean Monnet Saint-Étienne & CNRS, Laboratoire de Géologie de Lyon, Terre Planètes Environnement, UMR 5276, 69100 Villeurbanne, France

[2]Université de Paris, Institut de Physique du Globe de Paris, CNRS, F-75005, Paris, France

Correspondence to: Pascal Allemand (allemand@univ-lyon1.fr)

Abstract.

Rivers transports coarse sediment (gravel, cobbles, or boulder) as bedload. During a flood, when the discharge is high enough, the sediment grains move by rolling and bouncing on the river bed. Measuring bedload transport in the field is notoriously difficult. Here, we propose a new method to characterize bedload transport by floods. Using a drone equipped with a high resolution camera, we recorded yearly images of a bar of the Vieux-Habitants river, a gravel-bed river located on Basse-Terre Island (Guadeloupe, French West Indies). These images, combined with high frequency measurements of the river discharge, allow us to monitor the evolution of the population of boulders on the river bed. Based on this dataset, we estimate the smallest discharge that can move the boulders, and calculate the effective transport time of the river. We find that transport occurs about 10 hours per year. When plotted as a function of this effective transport time, likelihood of a given boulder remaining at the same location decreases exponentially, with an effective residence time of 17 hours. We then propose a rough estimate of the average number of boulders that the river carries every year.

1 Introduction

Rivers collect sediment from the surrounding hillslopes and carry it down to the oceans (Leopold et al., 1995). The resulting sediment flux is often intermittent: only during floods does the river exert on its bed force strong enough to move its sediment (Phillips and Jerolmack, 2014; Philipps et al., 2018). Flood after flood, and a river gradually exports sediment out of its catchment. The frequency of the floods and the quantity of sediment they transport thus set the erosion rate of the catchment (Wolman and Miller, 1960).

The fate of a particle entrained during a flood depends on its size. Fine sediments are carried in suspension. Coarse ones, conversely, travel as bedload: they roll, slip and bounce on the river bed, until they eventually settle down. This process is inherently stochastic (Einstein, 1937). A turbulent burst or a collision with a travelling grain can dislodge a particle from the bed (Charru et al., 2004; Ancey et al., 2008; Houssais and Lajeunesse, 2012). Once in motion, the particle's velocity fluctuates and its eventual deposition is, again, a random process (Lajeunesse et al., 2010; Furbish et al., 2012). Even in a steady flow, a

https://doi.org/10.5194/esurf-2021-77
Preprint. Discussion started: 10 November 2021

sediment particle idles on the bed most of the time; its journeys downstream (Lajeunesse et al., 2017). Overall, the combination of these stochastic events generates a downstream flux of sediment, referred to as "bedload transport", whose intensity depends on flow, and on the grain size density and shape (Einstein, 1950; Bagnold, 1973, 1977).

Bedload transport accounts for a large part of the sediment load exported out of mountainous catchments (Métivier et al., 2004; Meunier et al., 2006; Liu et al., 2008). It carves the channel of bedrock rivers, controls the shape and size of alluvial rivers, and generates ripples, dunes, bars and terraces (Gomez, 1991; Church, 2006; Seminara, 2010; Devauchelle et al., 2010; Aubert et al., 2016; Métivier et al., 2017; Dunne and Jerolmack, 2020; Abramian et al., 2020). In the field, geomorphologists measure bedload by collecting the moving particles in traps or baskets (Helley and Smith, 1971; Leopold and Emmett, 1976; Habersack et al., 2016). These direct measurements are laborious, and sometimes risky. These difficulties have motivated the development of alternative methods. One may, for example, estimate the intensity of bedload transport from the noise it generates (Burtin et al., 2008, 2011, 2014; Turowski and Rickenmann, 2009; Mao et al., 2016). However, the calibration of these sismic and acoustic proxies still requires direct measurements (Gimbert et al., 2014; Thorne, 2014; Burtin et al., 2016).

An alternative is to monitor the displacements of individual particles (Dietrich and Smith, 1984). These tracers – painted boulders or Radio Frequency Identification Passive Integrated Transponders (RFID PIT) inserted into the boulder– travel with the flow during floods (Cassel et al., 2020). Between two floods, however, one may look for the tracers on the exposed river bed. By repeating this procedure, one gradually reveals the trajectories of the tracers. Although laborious, this method provides reliable information, without perturbing the flow. Tracer particles have been used to evaluate the storage of particles in the sediment bed (Haschenburger and Church, 1998; Bradley, 2017), and to estimate the distance that a bedload particle travels before it settles down (Ferguson and Wathen, 1998; Martin et al., 2012). In large numbers, tracers form a plume, which disperses as it travels downstream (Bradley and Tucker, 2012; Phillips and Jerolmack, 2014). We can then infer the mean bedload flux from the deformation of this plume (Lajeunesse et al., 2018).

Measuring bedload transport, nonetheless, remains arduous, and some questions are still open. On average, how often can a river transport its coarsest sediment? How long does a boulder remain on the river bed? We address these questions with a new approach. Instead of tracking the particles when they travel, we monitor the evolution of their population at a fixed location. In that sense, our method can be called "Eulerian". Using a drone, we recorded yearly images of the bed of a tropical volcanic island (section 2), a gravel-bed river located in Basse-Terre Island (Guadeloupe, French West Indies). Combined with high frequency measurements of the river discharge, these images allow us (1) to follow the population of boulders that make up the bed, (2) to characterize the bedload transport in this river and its evolution over eight years (section 3). Finally, using these observations, we propose an estimate of the intensity of bedload transport averaged over a year, which include the contribution of hurricanes (section 4).

https://doi.org/10.5194/esurf-2021-77
Preprint. Discussion started: 10 November 2021

Earth Surface Dynamics Discussions
Open Access
EGU

2 Field site, measurement and processing

We conducted our investigation on Basse-Terre Island, a volcanic island of the Guadeloupe archipelago, which is part of the subduction arc of the Lesser Antilles (Feuillet et al., 2002 - Fig. 1a). The climate of Basse-Terre is tropical, with daily temperatures between 24 and 28 °C, and an average rainfall rate of about 5200 mm y^{-1}. Rains occur mainly as short and intense events. During the rainy season, which extends from June to January, storms and hurricanes are frequent, and the rainfall rate may reach up to 590 mm day^{-1}. As a result, the discharge of rivers varies abruptly, with frequent flash floods.

Rad et al. (2006) estimated the erosion rate of several Basse-Terre catchments, based on the chemical composition of the dissolved load. They found that it varies between 800 and 4000 t km^{-2} y^{-1}, or, equivalently, 0.3 and 1.5 mm y^{-1} (for a rock density of about 2900 kg m^{-3}). These values are consistent with the volume of sediment mobilized by landslides during extreme climatic events (Allemand et al., 2014). They place Basse-Terre Island amongst the fastest eroding places on Earth (Summerfield and Hulton, 1994). This observation led to the creation of the "Observatoire de l'Eau et de l'éRosion aux Antilles" (ObsERA), an observatory which monitors erosion within the French Network of Critical Zone Observatories (Gaillardet et al., 2018). Our field site is located the Vieux-Habitants catchment which is monitored by ObsERA.

The Vieux-Habitants river (Fig. 1b) drains a 30 km^2 watershed on the leeward side of the island. Most of the watershed, made of andesitic lava and pyroclastic deposits aged from 600 to 400 ky, is covered with a dense rain forest (Samper et al., 2007). The Vieux-Habitants river flows over 19 km, from its headwater at an altitude of 1300 m, down to the Vieux-Habitants village, where it discharges into the Caribbean Sea. The channel is made of bedrock, partly covered by a thin layer of alluvial sediment. Five kilometers from the sea, the river turns alluvial, and its slope gradually decreases. Our field site is a reach of the Vieux-Habitants river located 3 km from the sea, at an elevation 45 m a.s.l. There, the river bed is alluvial and the channel, confined between two steep banks about 2.5 m high, meanders. A large boulder bar, 300 meters long and 35 meters wide, occupies the inner side of the channel (Fig. 1c, d).

The *Direction de l'Environnement, de l'Aménagement et du Logement* (DEAL-Guadeloupe) operates a stream gauge, at the Barthole station, three kilometers upstream of our field site (Fig. 1b). This station has been measuring the river discharge every ten minutes for more than 15 years, except for an interruption between 2009 and 2011. As no major tributary joins the main stream between Barthole and our field site, we shall assume that the data acquired in Barthole provide a reasonable estimate of the river discharge at our site.

A statistical analysis of the data acquired between 2011 and 2018 reveals that the discharge stays below 10 m^3 s^{-1} during 90% of the time (Fig. 2a). In this low flow state, the boulder bar surfaces and the river flows in a channel that forms between the right side of the bar and the left bank of the river (Fig. 1d). There, the water depth is about 0.3 m, but may locally exceed 0.7 m (Fig. 1c, d). Floods are characterized by a steady increase of the discharge during 1 to 6 hours, followed by a recession that lasts typically 4 to 18 hours (Guérin et al., 2018). Although frequent, their intensity rarely exceeds 50 m (Fig. 2b): between 2011 and 2018, the river discharge stayed above 50 m^3 s^{-1} during 60 hours in total (Fig. 2a). The largest flood ever recorded in

https://doi.org/10.5194/esurf-2021-77
Preprint. Discussion started: 10 November 2021

Earth Surface Dynamics Discussions
Open Access
EGU

Barthole occurred during hurricane Maria, from September 18 to September 19, 2017. The water discharge then reached more than 250 $m^3 s^{-1}$, flooding not only the bar but also the river's banks. After the hurricane, the river returned to its normal course, along the right side of the bar.

To understand how floods affect the river bed, we acquired aerial images of our field site with a camera carried out in a hexacopter Unmanned Aerial Vehicle (DRELIO - *DRone hELIcoptere pour l'Observation de l'environnement*). This device, specially designed for tropical conditions, is capable of flying in steep watersheds, with dense vegetation and requires only a small takeoff area (Delacourt et al., 2009). We started working in 2011, with a Nikon D700 reflex camera, equipped with a 35 mm lens. In 2016, we replaced the camera with a Sony Alpha 7 reflex, still in use at present. As a result, the resolution of our images improved from 0.04 meters/pixel in 2011 to 0.02 meters/pixel starting from 2016.

From 2011 to 2018, we performed eight field campaigns and followed the same procedure. We flew DRELIO at an elevation of 80 m above the river bed, and used the on-board camera to acquire a series of images that covered the entire boulder bar. At this altitude, the overlap between two neighboring images is about 30 %. Four to six images are therefore enough to cover the whole bar. After each campaign, using a raster graphic editor, we drew the contours of the boulders visible on each image. The smallest grains visible on our images are 2 centimeters large. On the bar, however, most boulders have a diameter larger than 0.2 meters, and many are larger than 1 meter. In practice, we restricted our analysis to boulders with a diameter larger than 0.5 meters, as they are clearly distinguishable on the images. Using a Geographical Information Software (GIS), we vectorized the contours of these boulders and used a series of reference points to calibrate the scale of the resulting data. This method allowed us to calculate the exposed area of each boulder, A, from which we deduced its effective diameter, defined as the diameter D of a disk with the same surface area, $D = 2\sqrt{A/\pi}$.

Following this procedure, we produced a total of eight GIS, once per year from 2011 to 2018. Each GIS consisted in (1) a series of images of the bar warped around the image of the center of the bar, (2) the contours of the boulders of diameter larger than 0.5 m. Figure 3 shows a close view of two of these GIS, in the region of the bar delineated by the red rectangle in Fig. 1d. The first GIS was acquired in 2012 (Fig. 3, left) and the second one in 2013 (Fig. 3, right). In both cases, the flow in the river was low, and the water level, partly visible in the upper part of the images, was about the same. The comparison between these two GIS reveals some changes at the surface of the bar. Several boulders (yellow contours on Fig. 3), at repose on the bar in 2012, are not visible anymore in 2013: they have been entrained by the river, at some time between our two acquisition campaigns. Conversely, we also observe the appearance, in 2013, of several boulders that were not present in 2012 (red contours on Fig. 3): these boulders have been deposited on the bar, at some time between the acquisitions of the two images. Finally, the rest of the boulders (blue contours on Fig. 3) remained in place. The comparison between two consecutive GIS therefore allows us to identify the fate of each block. Based on this method, we attribute to each boulder contour, in each GIS, a label which specifies whether it was already in place during the previous campaign, or if it has been deposited recently. Some cases turn out to be ambiguous: a few boulders disappeared and then reappeared on more recent images, as floods covered them with sediment, before exposing them again. Those ambiguous cases were duly labelled and the corresponding boulders

https://doi.org/10.5194/esurf-2021-77
Preprint. Discussion started: 10 November 2021

Earth Surface Dynamics Discussions
Open Access
EGU

were considered immobile. Following this procedure, we end up with a dataset that contains the position and the size of all boulders larger than 50cm. We also know whether the boulder stayed in place or if, and when, it was deposited and/or entrained away. In short, we have turned the boulders into tracers. In the next section, we analyze this dataset to characterize the transport of boulders in the Vieux-Habitants river.

3 Results

3.1 Structure of the bar: mobile and consolidated layers

Our data show that entrained and deposited boulders are uniformly distributed over the whole bar. There is no particular place from which boulders would be preferentially exported, nor onto which they would be preferentially deposited. This suggests that, during floods, bedload transport is uniform over the bar.

We also observe the existence of two families of immobile boulders. Some of them were deposited at the surface of the bar during the course of our survey. They remained immobile for several years, until the river entrained them again. Others remained immobile during the whole survey. The latter are partially buried in a matrix of smaller sediment and appear to belong to a stable underlying base layer, that spans over the entire bar. This observation is consistent with laboratory experiments, in which a layer of mobile grains travels over a static sediment bed (Charru et al., 2004, Lajeunesse et al., 2010). Although mobile grains regularly settle on the static bed, the flow eventually dislodges them and set them back in motion. Based on these observations, we interpret our field data as the result of the existence of two layers of boulders: (i) a discontinuous surface layer of mobile boulders, and (ii) an underlying basal layer of static ones. In the following, we focus on the properties of the layer of mobile boulders.

3.2 Granulometric distribution

The size of the mobile boulders at the surface of the bar ranges from 0.5 to 2 meters. To characterize their distribution, we divide this interval into 6 uniform bins, and distribute the boulders in each one according to their size. We then compute the dimensionless surface density of each class *i*, defined as the number of grains per unit surface, normalized by the area of a grain:

$$\tilde{\sigma_i} = \frac{N_i \times \pi D_i^2}{S} \quad (1)$$

where N_i is the number of boulders in class *i*, D_i is their effective diameter, and S=2000 m^2 is the area of the bar. The dimensionless surface density σ_i can also be interpreted as the proportion of the bar area occupied by the boulders of class *i*.

The number of boulders in each class and the corresponding surface density vary from year to year. To account for these variations, we compute these two quantities for each field campaign, and represent the results with a box plot (Fig. 4a). We find that the surface density does not change significantly with time: in each class, its variations are negligible with respect to

https://doi.org/10.5194/esurf-2021-77
Preprint. Discussion started: 10 November 2021

Earth Surface Dynamics Discussions
Open Access
EGU

the median value. This suggests that, at first order, the size distribution of the boulders is in steady state. The surface density, however, rapidly decreases with grain size (Fig. 4a). Boulders within 0.5 and 0.75 m in diameter – named D_1 thereafter - dominate the surface of the bar, at least in the range of diameters accessible to our measurement method. For this class, the median value of the dimensionless surface density is $\tilde{\sigma} = 0.055$. Returning to dimensional quantities, this corresponds to a surface density of $\sigma = 0.23$ boulders m^{-2}, or, equivalently, a total number of about 600 boulders over the 2000 m^2 of the bar.

That the size distribution of the boulders is almost in steady state is an unexpected observation. To understand it, we distinguish, within each class, the boulders freshly deposited (Fig. 4a, green boxes) from those that were already in place during the preceding campaign (Fig. 4a, yellow boxes), and calculate their surface density. The result varies within boulder size (Fig. 4a). Each year, about half of the population of D_1 boulders is made up of freshly deposited sediment (Fig. 4a). In this class, the boulders are highly mobile, but the number of boulders entrained by floods balances, on average, the number of fresh boulders deposited on the bar, thus maintaining their surface density (Fig. 4b).

This is not true for larger boulders. Indeed, the proportion of freshly deposited boulders rapidly decreases with the grain size, and eventually vanishes for boulders larger than 1.75 meters (Fig. 4a). The mobility of a boulder thus decreases with its size. It is because large boulders are seldom mobilized that their surface density remains constant in our dataset. We thus cannot assess whether their population is effectively in steady state.

Given that the D_1 boulders are, at the same time, the most abundant and the most mobile, we shall now concentrate our analysis on this class of boulders. In the next section, we start by estimating the threshold discharge necessary to entrain them.

3.3 Threshold for the initiation of transport

The boulders of our field site move only when the discharge of the Vieux-Habitants river is large enough. Based on our 8 GIS, we identify the largest boulders deposited on, or entrained from, the bar between two consecutive campaigns. We then plot their diameter as a function of the maximum water discharge between the campaigns (Fig. 5). We find that the size of these boulders correlates well with the maximum discharge. Assuming that the largest boulders are transported when the discharge is at its highest, the resulting curve provides a reasonable estimate of the threshold discharge beyond which transport takes place, as a function of grain size, for boulders larger than about 0.8 m. The lack of data, however, does not allow us to constrain the threshold discharge of smaller boulders. Instead, we shall now try to evaluate it, by extrapolating our observations in terms of dimensionless quantities.

In practice, the threshold discharge corresponds to the discharge for which the shear stress exerted by the river on its bed exceeds a critical value (Shields, 1936). The instantaneous turbulent stress exerted on the river bed is, however, highly variable in space and in time: it depends on the flow, on the shape of the channel, on the river slope, on the bed roughness, and its measurement in the field is challenging (Henderson 1963, Parker 1978, Chauvet et al., 2014, Métivier et al., 2017, Nezu and H. Nakagawa, 1993). Here, to simplify the problem, we assimilate the river to a rectangular channel of width *W*, depth *H*, and

https://doi.org/10.5194/esurf-2021-77
Preprint. Discussion started: 10 November 2021

Earth Surface Dynamics Discussions
Open Access
EGU

slope *S*. Based on the Darcy-Weisbach equation, we then derive the threshold discharge required to transport a boulder (see appendix for a full derivation):

$$Q_c = W \frac{D^{3/2}}{S} \left(\Theta_c \frac{\Delta\rho}{\rho}\right)^{3/2} \left(\frac{g}{C_f}\right)^{1/2} \quad (2)$$

where $\Delta\rho = \rho_s - \rho$ is the difference between the density of rock and that of water, C_f is the Darcy-Weisbach friction parameter, g is the acceleration of gravity, and Θ_c is the threshold Shields parameter (Shields, 1936). Our model is crude and some of the parameters in equation (2) are difficult to estimate. Based on direct field measurements, we estimate the river width to be W=30 m. Using the DEM, we calculate its average slope and find to be about S = 0.03. We use the value Θ_c= 0.02 for the threshold Shields number (Shields, 1936). The most inaccurate of our parameters is certainly the friction coefficient for which we use the value C_f = 0.1, typical in mountain streams (Limerinos, 1970). Despite these shortcomings, equation (2) reasonably accounts for our observations (Fig. 5). Encouraged by this result, we use equation (2) to calculate the threshold discharge of D_1 boulders. We find a threshold discharge between 38 and 52 m^3s^{-1}, with a medium value of 45 m^3s^{-1}. In the next section, we use this value to estimate the time during which the river effectively transports these boulders.

3.4 Effective transport time

In the previous section, we calculated that D_1 boulders move only when the river discharge exceeds about 45 m^3 s^{-1}. Based on this result, we now evaluate the effective transport time, defined as the cumulated time that the river spends above this threshold (Fig. 6). We find that the effective transport time amounts to 85 hours over the period 2011 to 2018. The proportion time during which the river is above the entrainment threshold is I= 0.12%. On average, these boulders thus move during about 10 hours each year.

The effective transport time depends on the occurrence of floods, and therefore, on the distribution of rainfalls. As the latter varies from year to year, so does the effective transport time (Fig. 6): the river spent less than 5 hours above threshold between 2014 and 2016 (an unusually dry period). Conversely, it spent 32 hours above the threshold between 2017 to 2018, a period that includes the hurricane Maria. Even then, the effective transport time did not exceed 0.36% of the total time that is about 30 hours each year. On a tropical volcanic island like Guadeloupe, the boulders move only during short periods, whose cumulated duration depends on the frequency and the intensity of the storms that hit its catchments.

3.5 Evolution of the population of boulders

So far, we focused on mobile boulders, their threshold of transport, and their effective transport time. We now use our data to document the evolution of their population. To do so, we start from the 2011 GIS and identify all the D_1 boulders that are at idle on the bar. Using later images, we then monitor the evolution of this population. We find that their number decreases with the effective transport time, as they are progressively entrained by floods, and replaced with new boulders (Fig. 7).

https://doi.org/10.5194/esurf-2021-77
Preprint. Discussion started: 10 November 2021


Earth Surface Dynamics Discussions

We repeat the same procedure with the boulders that first appeared in 2012, and in the following years until 2017. By doing so, we monitor seven populations in total. To compare their evolution, we normalize the number of boulders in each population with its initial value, and plot the result as function of the effective transport time (Fig. 7). We find that all data points gather around the same trend: the number of boulders decreases rapidly at first. With time, however, the rate slows down gradually.

For a given boulder size, the surface density is small (σ =0.23 boulder m^{-2} - see section 3.2), and we expect little interaction between them during transport. Following Einstein (1937) and Charru et al. (2004), we thus assume that the number of boulders that leave the bar is proportional to the number of boulders available on its surface, that is:

$$\frac{dN}{dt} = -\frac{N}{\tau} \quad (3)$$

where t is the effective transport time, N is the number of boulders on the bar surface at time t, and τ is the characteristic entrainment time. The solution of Eq. (3), $N = N_0\, e^{-t/\tau}$, is a decaying exponential, of characteristic time τ, where N_0 is the initial number of boulders. Fitting this solution to our data yields a good representation of the evolution of N (R^2 =0.84). We find a characteristic time τ =17 hours (Fig. 7).

The model proposed here is simplistic. It does not take into account the water flow variations during a floods, and relies on a crude description of the threshold of transport. Yet, the exponential decrease of an initial population of boulders is consistent with the data plotted on figure 7, and we therefore expect that the value of the characteristic time τ is a reasonable estimate of the residence time of boulders on the bar, expressed in terms of the effective sediment transport time. The characteristic time during which a D_1 boulder stays at rest on the bar is surprisingly short. Expressed in terms of half-life, this means that it takes an effective transport time of log2 τ = 12 hours to entrain half of the boulders initially present on the bar, and to replace them with new ones.

4 Boulder discharge

Based on the model of previous section, we now estimate the boulder discharge in the Vieux-Habitants river. Once again, we assimilate the river to a rectangular channel. During a flood, the water discharge is above the threshold of entrainment, and the flow continuously entrains new boulders. Laboratory experiments show that, once dislodged from the bed, bedload particles travel over a characteristic flight length, L_f, before they are deposited on the bed (Lajeunesse et al., 2010; Furbish et al, 2012, 2016). If this result holds in nature, the discharge of boulders across a given section of the river is just the number of grains entrained per unit time, in a bed area of size WL_f (Fig. 8). According to equation (4), boulder discharge is therefore the number of boulders at rest on this surface, $\sigma W L_f$, divided by their residence time, τ, where σ is the surface density of boulders (Einstein, 1937). Following this reasoning, we find that the volumetric discharge of boulders reads:

$$Q_e = \frac{\pi D^3}{6} \times \frac{\sigma W L_f}{\tau}, \quad (4)$$

where we assimilate the boulders to spheres of diameter D.

https://doi.org/10.5194/esurf-2021-77
Preprint. Discussion started: 10 November 2021

Earth Surface Dynamics Discussions
Open Access
EGU

Equation (4) yields the instantaneous boulder discharge in terms of the effective transport time. To convert this value into an annual sediment flux, we multiply it by the proportion of time, *I*, during which the river is above the entrainment threshold:

$$Q_y = I \times \frac{\pi D^3}{6} \times \frac{\sigma W L_f}{\tau} \quad (5)$$

To calculate the sediment discharge, we need to estimate all the parameters in equation (5). In the previous sections, we found that, for D_1 boulders, the surface density is $\sigma = 0.23$ boulders m^{-2}, the residence time is $\tau = 17$ h, and the proportion of effective transport time is $I = 0.12\%$. To calculate the discharge, we still need to evaluate the average flight length of a boulder. Unfortunately, our measurement method does provide the trajectories of the boulders, and we thus do not have any direct measurement of their flight length. Instead, we propose a lower bound for it. During our survey, several uncommonly large boulders, of size larger than 1.5 m, disappeared from the bar. They have been entrained by a flood, between two successive campaigns. Although these boulders were large enough to be identifiable, we never detected them again. We therefore conclude that their flight length must be longer than the length of the bar, that is $L_f \gtrsim 300$ m. Based on this value, and assuming that bedload is transported across the entire river, we find a boulder discharge of 8 m^3 per hour of effective transport time, which corresponds to an annual sediment discharge $Q_y = 61$ m^3 y^{-1}, or equivalently, 177 t y^{-1} for a rock density of 2900 kg m^{-3}.

So far, we have restricted our analysis to boulders between 0.5 and 0.75 m (D_1 boulders). We now extend our calculations to larger boulders. To do so and for lack of direct measurements, we assume that the flight length and the residence time τ do not vary much with the boulder size. We then compute the threshold discharge of large boulders from equation (2), calculate the proportion of time, I, during which they are transported, and estimate their annual discharge from equation (5) (see table 1). We find that the D_1 population dominates the total solid load, whereas the contribution of boulders larger than 1 m is marginal. In total, the discharge of boulders in the Vieux-Habitants river amounts to about $Q_y = 76$ m^3 y^{-1}, that is 240 t y^{-1} from boulders between 0.5 to 2 m.

It might be tempting to extrapolate our results to boulders and pebbles smaller than 0.5 meters. This would, however, be a precarious endeavor: the detection of small boulders proved difficult on our images, and we do not have any access to their effective transport time. Besides, small boulders are probably sensitive to the bed roughness, and extrapolating their threshold discharge or their flight length from those of large boulders would be hazardous (Mao et al., 2014).

5. Conclusion

To the best of our knowledge, we present the first attempt at characterizing bedload transport based on yearly UAV image acquisition. Despite — or, maybe, owing to — its simplicity, the method proves robust: the comparison of images taken one year apart allowed us to monitor the evolution of the population of boulders at the surface of the Vieux-Habitants river. Using high frequency measurements of the river discharge, it was then possible to determine the threshold discharge necessary to set boulders in motion, and estimate the time during which the flow was strong enough to transport them. In the Vieux-Habitants

https://doi.org/10.5194/esurf-2021-77
Preprint. Discussion started: 10 November 2021

river, this effective transport time amounts to 10.5 hours per year, on average. The transport of boulders is therefore a rare event. The effective transport time depends on the time distribution of rainfalls, which fluctuates from year to year. In a river like the Vieux-Habitants river, it is therefore necessary to consider the effective transport time to evaluate bedload transport.

Einstein (1937) was the first to propose that the entrainment of bedload particles is inherently a random process. This hypothesis is at the core of the entrainment-deposition model (Charru et al., 2004; Lajeunesse et al., 2010; 2018). When expressed in terms of the effective transport time, our data are consistent with this assumption: the population of boulders on the bed of the Vieux-Habitants river decreases exponentially, as expected for a random Poisson process. The characteristic time of this decay — in fact, the residence time of the boulders on the bed — is surprisingly short: τ =17 hours of effective transport time, distributed aver about 2 years of actual time.

Based on our observations, we evaluate the annual discharge of boulders in the Vieux-Habitants river to be about Q_y = 240 t y^{-1}. When rescaled to the area of the Vieux-Habitants watershed, the resulting erosion rate, 8 t km^{-2} y^{-1}, is very small with respect to the 800 to 4000 t km^{-2} y^{-1} estimated from a geochemical mass balance or a geometrical reconstruction (Rad et al., 2006; Samper et al., 2007). This suggests that the solid load exported out the catchment primarily consists of sediment smaller than 0.5 m. Given the intensity of the weathering rates in Basse-Terre island, it is likely that most of the solid load is, in fact, made of fine regolith, carried in suspension in the flow.

Finally, our estimate of the boulder discharge is based on a rough lower bound of flight length. Direct measurements of this length remain an instrumental challenge to this day.

Code/Data availability

Discharge data used for figures 2 and 6 are available on http://www.hydro.eaufrance.fr/. UAV Images and dataset are available on Harvard Dataverse https://dataverse.harvard.edu/dataset.xhtml?persistentId=doi:10.7910/DVN/QRHM8E

Author contributions

PA designed and performed the field measurements, and processed the resulting data. All the authors developed the overall ideas and were responsible for critical contributions, passing the final manuscript and editing text and figures.

Competing interests.

The authors declare no competing interests.

https://doi.org/10.5194/esurf-2021-77
Preprint. Discussion started: 10 November 2021

Acknowledgements

This work was carried out in the framework of Obsera (Observatoire de l'Eau et de l'Erosion aux Antilles). Obsera is part of OZCAR infrastructure. P. Grandjean, S. Passot, V. Robert et T. Kitou are warmly thanked for their efficiency and involvement in this work. This is IPGP contribution n°

Appendix A - Threshold discharge

Here, we estimate the threshold discharge above which the river can transport its sediment. To do so, we assimilate the channel to a rectangle of width W, depth H, and slope S. The Darcy-Weisbach equation then relates the average flow velocity V to the shear stress τ exerted on the river bed (Limerinos, 1970):

$$\tau = C_f \rho V^2 \quad \text{(A1)}$$

where ρ is the density of water and C_f is the Darcy-Weisbach friction coefficient. In steady state channel flow, the momentum balance requires that:

$$\tau = \rho g S H. \quad \text{(A2)}$$

At the onset of sediment motion, the Shield number, Θ, defined as the ratio between the driving force acting on the grains and the weight of a grain, must equal a threshold value Θ_c:

$$\Theta = \frac{\tau}{\Delta \rho g D} = \Theta_c, \quad \text{(A3)}$$

where Δρ is the difference between the density of a grain and that of water, g, is the acceleration of gravity, and D is the grain size. Combining (A2) with (A3) yields the expression of the flow depth H at the threshold of entrainment:

$$H = \Theta_c \frac{\Delta \rho}{\rho} \frac{D}{S}. \quad \text{(A4)}$$

Similarly, combining (A1) with (A2) and (A5) yields the average flow velocity at the threshold of entrainment:

$$V = \left(\Theta_c \frac{\Delta \rho}{\rho} \frac{gD}{C_f} \right)^{1/2}. \quad \text{(A5)}$$

Injecting the velocity and the flow depth into the expression of the water discharge, $Q = WHV$, we find the threshold discharge above which the river can transport a boulder of diameter D:

$$Q_c = W \frac{D^{3/2}}{S} \left(\Theta_c \frac{\Delta \rho}{\rho} \right)^{3/2} \left(\frac{g}{C_f} \right)^{1/2} \quad \text{(A7)}$$

This expression, of course, is only a crude estimate, if only because the river is not a straight rectangular channel. Nonetheless, it provides a decent approximation of the flow conditions that are necessary to initiate the transport of a given class of boulders (Figure 5).

https://doi.org/10.5194/esurf-2021-77
Preprint. Discussion started: 10 November 2021

References

Abramian, A., Devauchelle, O., and Lajeunesse, E.: Laboratory rivers adjust their shape to sediment transport, Physical Review E, 102, 053 101, 2020.

Allemand, P., Delacourt, C., Lajeunesse, E., Devauchel, O., and Beauducel, F.: Erosive effects of the storm Helena (1963) on Basse Terre Island (Guadeloupe — Lesser Antilles Arc), Geomorphology, doi:10.1016/j.geomorph.2013.09.020, 2014.

Ancey, C., Davison, A., Bohm, T., Jodeau, M., and Frey, P.: Entrainment and motion of coarse particles in a shallow water stream down a steep slope, J. Fluid Mech., 595, 83–114, doi:10.1017/S0022112007008 774, 2008.

Aubert, G., Langlois, V.J., Allemand, P.: Bedrock incision by bedload: insights from direct numerical simulations, Earth Surf. Dynam., 4, 327–342, doi: 10.5194/esurf-4-327-2016, 2016.

Bagnold, R.: The nature of saltation and of Bedload transport in water, Proc. R. Soc. Lond., A 332, 473–504, 1973.

Bagnold, R.: Bedload transport by natural rivers, Water Resources Research, 13, 303–312, 1977.

Bradley, D. N.: Direct Observation of Heavy-Tailed Storage Times of Bedload Tracer Particles Causing Anomalous Superdiffusion, Geophysical Research Letters, 44, 2017.

Bradley, D. N. and Tucker, G. E.: Measuring gravel transport and dispersion in a mountain river using passive radio tracers, Earth Surface Processes and Landforms, 37, 1034–1045, 2012.

Burtin, A., Bollinger, L., Vergne, J., Cattin, R., and Nábelek, J.: Spectral analysis of seismic noise induced by rivers: A new tool to monitor spatiotemporal changes in stream hydrodynamics, Journal of Geophysical Research: Solid Earth, 113, 2008.

Burtin, A., Cattin, R., Bollinger, L., Vergne, J., Steer, P., Robert, A., Findling, N., and Tiberi, C.: Towards the hydrologic and bedload monitoring from high-frequency seismic noise in a braided river: The “torrent de St Pierre”, French Alps, Journal of hydrology, 408, 43–53, 2011.

Burtin, A., Hovius, N., McArdell, B., Turowski, J., and Vergne, J.: Seismic constraints on dynamic links between geomorphic processes and routing of sediment in a steep mountain catchment, Earth Surface Dynamics, 2, 21–33, 2014.

Burtin, A., Hovius, N., and Turowski, J. M.: Seismic monitoring of torrential and fluvial processes, Earth Surface Dynamics, 4, 285–307, 2016.

https://doi.org/10.5194/esurf-2021-77
Preprint. Discussion started: 10 November 2021

Cassel, M., Piegay, H., Fantino, G., Lejot, J., Bultingaire, L., Michel, K. and Perret, F.: Comparison of ground-based and UAV a-UHF artificial tracer mobility monitoring methods on a braided river, Earth Surface Processes and Landforms, 5, 1123-1140, doi: 10.1002/esp.4777, 2020.

Charru, F., Mouilleron, H., and Eiff, O.: Erosion and deposition of particles on a bed shared by a viscous flow, Journal of Fluid Mech., 519, 55–80, doi:10.1017/S0022112004001028, 2004.

Chauvet, H., Devauchelle, O., Métivier, F., Lajeunesse, E., and Limare, A.: Recirculation cells in a wide channel, Phys. Fluids (1994-present), 26, 016604, 1–10, 2014.

Church, M.: Bed material transport and the morphology of alluvial river channels, Annu. Rev. Earth Planet. Sci., 34, 325–354, 2006.

Delacourt, C., Allemand, P., Jaud, M., Grandjean, P., Deschamps, A., Ammann, J., Cuq, V., and Suanez, S.: DRELIO: An unmanned helicopter for imaging coastal areas, SI 56, Proceedings of the 10th International Coastal Symposium), 1489-1493, Lisbon, Portugal, 2009.

Devauchelle, O., Malverti, L., Lajeunesse, E., Lagrée, P., Josserand, C., and Thu-Lam, K.: Stability of bedforms in laminar flows with free surface: from bars to ripples, Journal of Fluid Mechanics, 642, 329–348, doi:10.1017/S0022112009991790, 2010.

Dietrich,W. and Smith, J.: Bedload Transport in a River Meander, Water Resources Research, 20, 1984.

Dunne, K. B. and Jerolmack, D. J.: What sets river width? Science advances, 6, eabc1505, 2020.

Einstein, H.: The bed-load function for sediment transportation in open channel flows, US Department of Agriculture. Soil Conservation Service, 1950.

Einstein, H. A.: Bedload transport as a probability problem, in: Sedimentation: 746 Symposium to Honor Professor H.A. Einstein, 1972. translation from 747 German of H.A. Einstein doctoral thesis. Originally presented to Federal Institute of Technology, Zurich, Switzerland, 1937, pp. C1 – C105, 1937.

Ferguson, R. and Wathen, S.: Tracer-pebble movement along a concave river profile: Virtual velocity in relation to grain size and shear stress, Water Resources Research, 34, 2031–2038, 1998.

Feuillet, N., Manighetti, I., and Tapponnier, P.: Arc parallel extension and localization of volcanic complexes in Guadeloupe, Lesser Antilles. J. Geophys. Res. 107, 1-29, doi:10.1029/2001JB000308, 2002.

https://doi.org/10.5194/esurf-2021-77
Preprint. Discussion started: 10 November 2021

Furbish, D., Roseberry, J., and Schmeeckle, M.: A probabilistic description of the bedload sediment flux: 3. The particle velocity distribution and the diffusive flux, Journal of Geophysical Research, 117, F03 033, 2012.

Furbish, D. J., Fathel, S. L., Schmeeckle, M. W., Jerolmack, D. J., and Schumer, R.: The elements and richness of particle diffusion during sediment transport at small timescales, Earth Surface Processes and Landforms, 2016.

Gaillardet, J., I. Braud, F. Hankard, S. Anquetin, O. Bour, N. Dorfliger, et al.: OZCAR: The French network of critical zone observatories. Vadose Zone J. 17:180067, doi:10.2136/vzj2018.04.0067, 2018.

Gimbert, F., Tsai, V. C., and Lamb, M. P.: A physical model for seismic noise generation by turbulent flow in rivers, Journal of Geophysical Research: Earth Surface, 119, 2209–2238, 2014.

Gomez, B.: Bedload transport, Earth-Science Reviews, 31, 89–132, 1991.

Guerin, A., Devauchelle, O., Robert, V., Kitou, T., Dessert, C., Quiquerez, A., et al.: Stream-discharge surges generated by groundwater flow. Geophysical Research Letters, 46, 7447–7455. doi:10.1029/2019GL082291, 2019.

Habersack, H., Kreisler A., Rindler R., Aigner J., Seitz, H., Liedermann, M., Laronne, J.B.: Integrated automatic and continuous bedload monitoring in gravel bed rivers, Geomorphology (2016), doi:10.1016/j.geomorph.2016.10.020, 2016.

Haschenburger, J. K. and Church, M.: Bed material transport estimated from the virtual velocity of sdiment, Earth Surface Processes and Landforms, 23, 791–808, 1998.

Helley, E. J. and Smith, W.: Development and calibration of a pressure-difference bedload sampler, Geological Survey Open-File Report, December 3, 1971., 1971.

Henderson, F. M.: Stability of alluvial channels, T. Am. Soc. Civ.Eng., 128, 657–686, 1963.

Houssais, M. and Lajeunesse, E.: Bedload transport of a bimodal sediment bed, J. Geophys.Res.-Earth, 117, doi: 10.1029/2012JF002490, 2012.

Lajeunesse, E., Malverti, L., and Charru, F.: Bedload transport in turbulent flow at the grain scale: experiments and modeling, J. Geophys. Res, 115, F04 001, doi:10.1029/2009JF001 628, 2010.

Lajeunesse, E., Devauchelle, O., Lachaussée, F., and Claudin, P.: Bedload Transport in Laboratory Rivers: The Erosion–Deposition Model, chap. 15, pp. 415–438, John Wiley & Sons Ltd., 2017.

https://doi.org/10.5194/esurf-2021-77
Preprint. Discussion started: 10 November 2021

Lajeunesse, E., Devauchelle, O., and James, F.: Advection and dispersion of bedload tracers, Earth Surface Dynamics, 5, 389–399, 2018.

Leopold, L. B. and Emmett, W. W.: Bedload measurements, East 85 Fork River, Wyoming, Proceedings of the National Academy of Sciences, 73, 1000–1004, 1976.

Limerinos, J.T.: Determination of the Manning coefficient from measured bed roughness in natural channels. United States, Geological Survey, Water-Supply Paper 1898-B, 1970.

Liu, Y., Metivier, F., Lajeunesse, E., Lancien, P., Narteau, C., and Meunier, P.: Measuring bedload in gravel bed mountain rivers: Averaging methods and sampling strategies, Geodin. Acta, 21, 81–92, https:// 10.3166/ga.21.81-92, 2008.

Mao, L., Carrillo R, Escauriaza C, Iroume A.: Flume and field-based calibration of surrogate sensors for monitoring bedload transport. Geomorphology, 253, 10–21. doi: 10.1016/j.geomorph.2015.10.002, 2016.

Martin, R. L., Jerolmack, D. J., and Schumer, R.: The physical basis for anomalous diffusion in bedload transport, Journal of Geophysical Research, 117, F01 018, 2012.

Métivier, F., Meunier, P., Moreira, M., Crave, A., Chaduteau, C., Ye, B., and Liu, G.: Transport dynamics and morphology of a high mountain stream during the peak flow season: the Ürümqi river (Chinese Tian-Shan), in: Second international conference on fluvial hydraulics - River flow 2004, 2004.

Métivier, F., Lajeunesse, E., and Devauchelle, O.: Laboratory rivers: Lacey's law, threshold theory, and channel stability, Earth Surface Dynamics, 5, 187, 2017.

Meunier, P., Metivier, F., Lajeunesse, E., Meriaux, A.S., and Faure, J.: Flow pattern and sediment transport in a braided river: The "torrent de St Pierre" (French Alps), J. Hydrol., 330, 496–505, 2006.

Nezu, I and Nakagawa, H.: Turbulence in Open Channel Flows. IAHR Monograph, A. A. Balkema, Rotterdam, 1993.

Parker, G.: Self-formed straight rivers with equilibrium banks and mobile bed. Part 1. The sand-silt river, J. Fluid Mech., 89, 109–125, 1978.

Phillips, C.B., and Jerolmack, D.J.: Dynamics and mechanics of tracer particles, Earth Surf. Dynam. Discuss., 2, 429–476, doi: 10.5194/esurfd-2-429-2014, 2014.

https://doi.org/10.5194/esurf-2021-77
Preprint. Discussion started: 10 November 2021

Phillips, C., Hill, K., Paola, C., Singer, M., and Jerolmack, D.: Effect of flood hydrograph duration, magnitude, and shape on bedload transport dynamics, Geophysical Research Letters, 45, 8264–8271, 2018.

Rad, S., Louvat, P., Gorge, C., Gaillardet, J., and Allègre, C.J.: River dissolved and solid loads in the Lesser Antilles: new insight into basalt weathering processes. J. Geochem. Explor. 88, 308-312, doi: 10.1016/j.gexplo.2005.08.063, 2006.

Samper, A., Quidelleur, X., Lahitte, P., and Mollex, D.: 2007. Timing of effusive volcanism and collapse events within an oceanic arc island: Basse-Terre, Guadeloupe archipelago (Lesser Antilles Arc). Earth Planet. Sci. Lett. 258, 175–191, doi:10.1016/j.epsl.2007.03.030, 2007.

Seminara, G.: Fluvial sedimentary patterns, Annual Review of Fluid Mechanics, 42, 43–66, 2010.

Summerfield, M. A., and Hulton, N. J.: Natural controls of fluvial denudation rates in major world drainage basins, J. Geophys. Res., 99(B7), 13871–13883, doi:10.1029/94JB00715, 1994.

Thorne, P.: An overview of underwater sound generated by interparticle collisions and its application to the measurements of coarse sediment bedload transport, Earth Surface Dynamics, 2, 531–543, 2014.

Turowski, J. M. and Rickenmann, D.: Tools and cover effects in bedload transport observations in the Pitzbach, Austria, Earth Surface Processes and Landforms, 34, 26–37, 2009.

Wolman, M. G. and Miller, J. P.: Magnitude and frequency of forces in geomorphic processes, The Journal of Geology, 68, 54–74, 1960.

https://doi.org/10.5194/esurf-2021-77
Preprint. Discussion started: 10 November 2021

Earth Surface Dynamics Discussions
Open Access
EGU

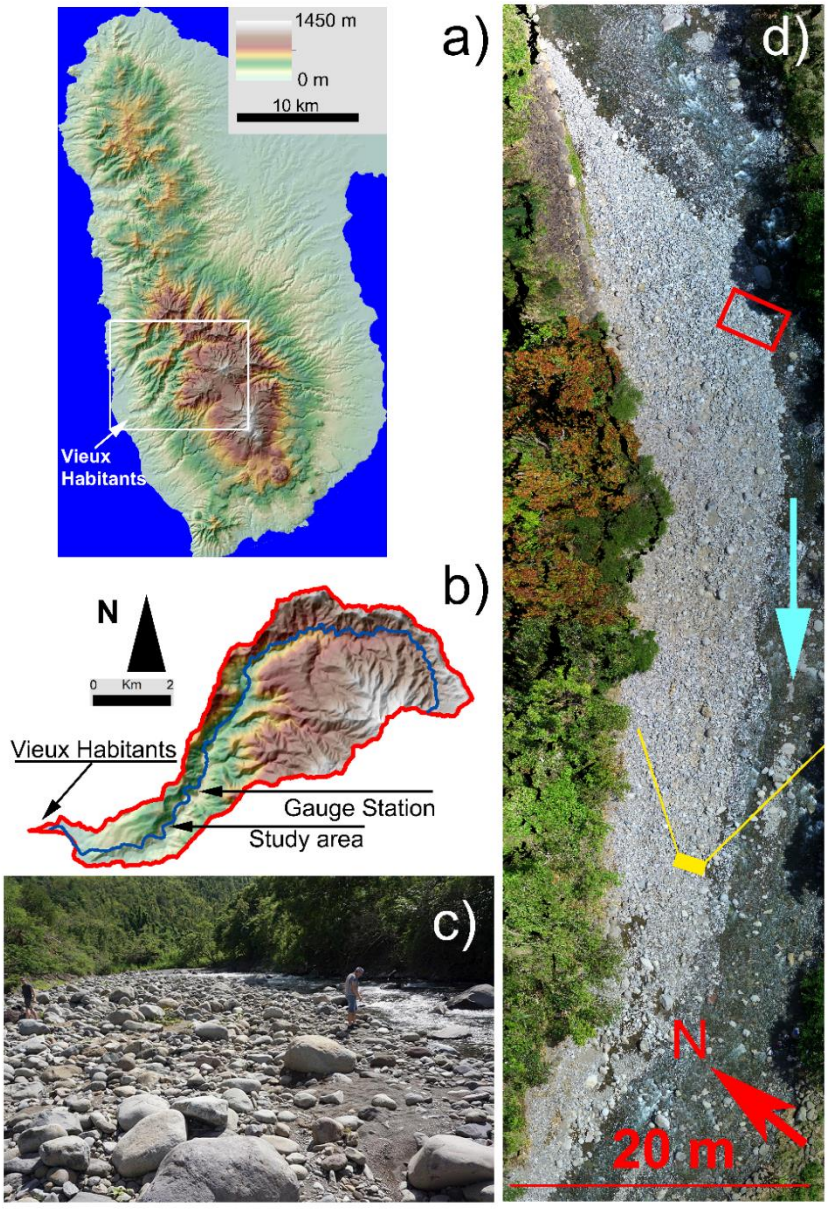

Figure 1: a) Basse Terre island in the Guadeloupe archipelago. The island separates the Atlantic Ocean in the East from the Caribbean Sea in the West. The white rectangle shows the position of the map displayed in b). b) The Vieux-Habitants river is located on the Caribbean side of Basse Terre. The watershed of Vieux-Habitants has an area of 19 km^2. The length of the river is 19 km. The water discharge is measured each 10 minutes at Barthole gauge station. The study area is located 2 km downstream of Barthole. c) A view of the bar from ground looking upstream shows the size of the boulders and their heterometric distribution. The two people give the scale. d) The area of interest. The bar is about 300 m long and 15 to 35 m wide. It lies on the right side of the river 3 km upstream of the seashore. In fair weather conditions, the bar is bounded on its left by the channel of the river which is 5 to 10 m wide and less than 1 m deep. The boulder bar is flooded 1 to 3 times a year. The red square shows the location of Fig. 3. The position of the camera and the field of view of c) is shown in yellow. The flow direction is given by the turquoise arrow.

https://doi.org/10.5194/esurf-2021-77
Preprint. Discussion started: 10 November 2021

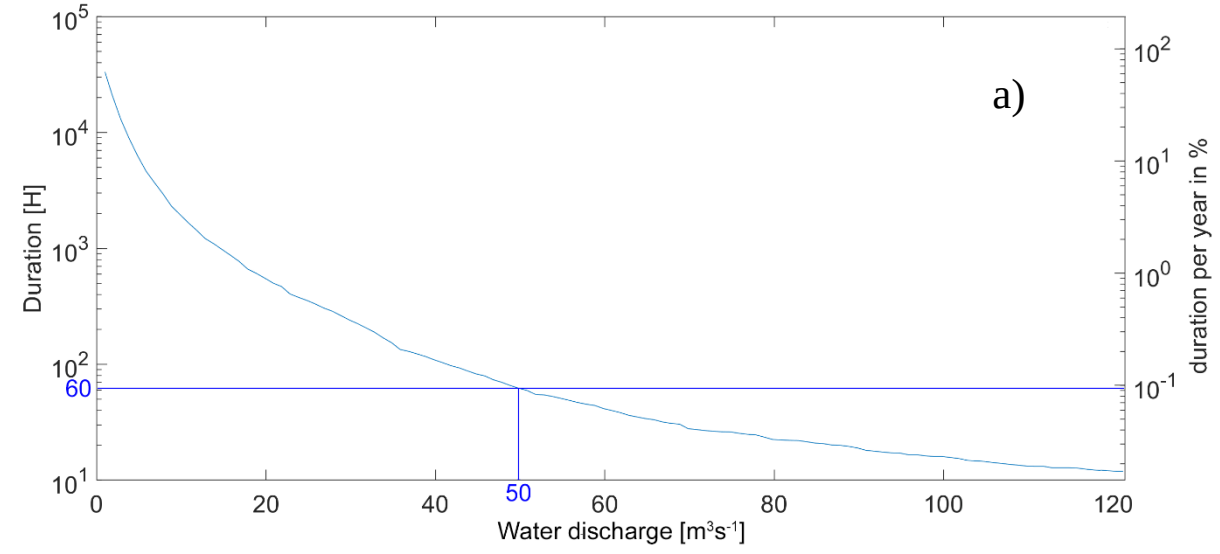

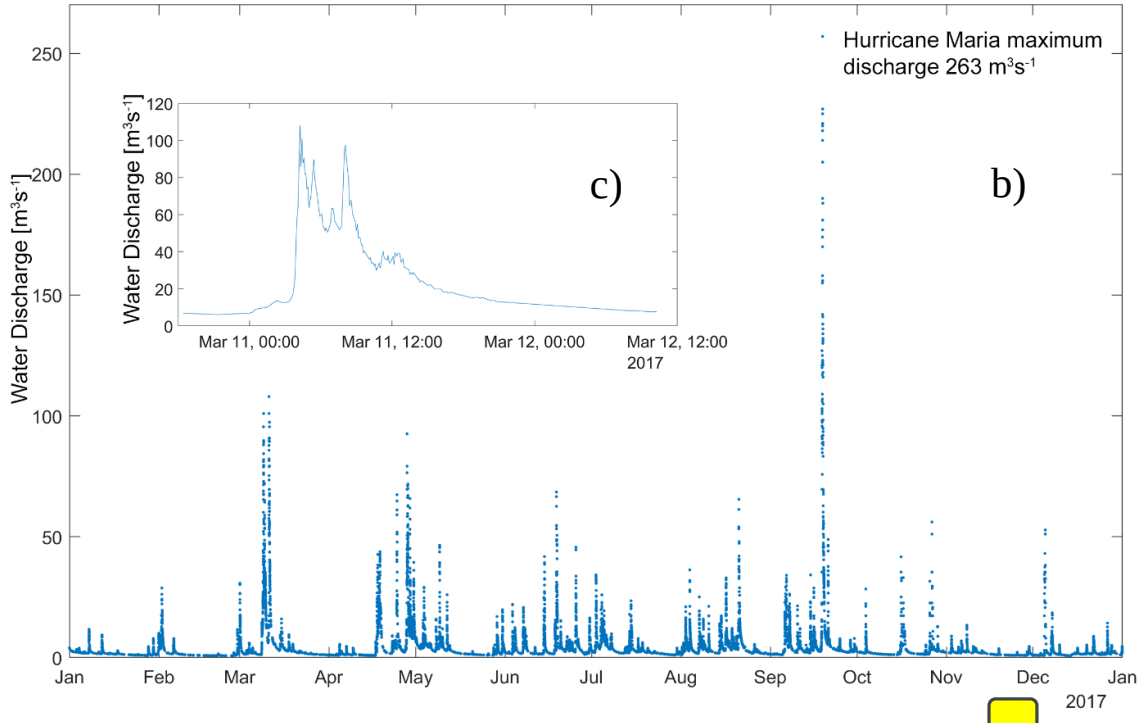

Figure 2: a) Duration of the water discharge above a given threshold from 2011 to 2018. A flow of 50 $m^3 s^{-1}$ was exceeded around 60 hours during the 8 years of measurement (about 0.1% of the total time). b) Hydrograph of year 2017. In low flow conditions, that is most of the time, the discharge is less than 5 $m^3 s^{-1}$. The largest discharge recorded in 2017 was 263 $m^3 s^{-1}$. It was reached on September 19 during hurricane Maria. c) The inset shows a typical flood. The water discharge reaches its maximum in less than one hour. The peak of the flow is followed by a slow recession toward low flow.

https://doi.org/10.5194/esurf-2021-77
Preprint. Discussion started: 10 November 2021

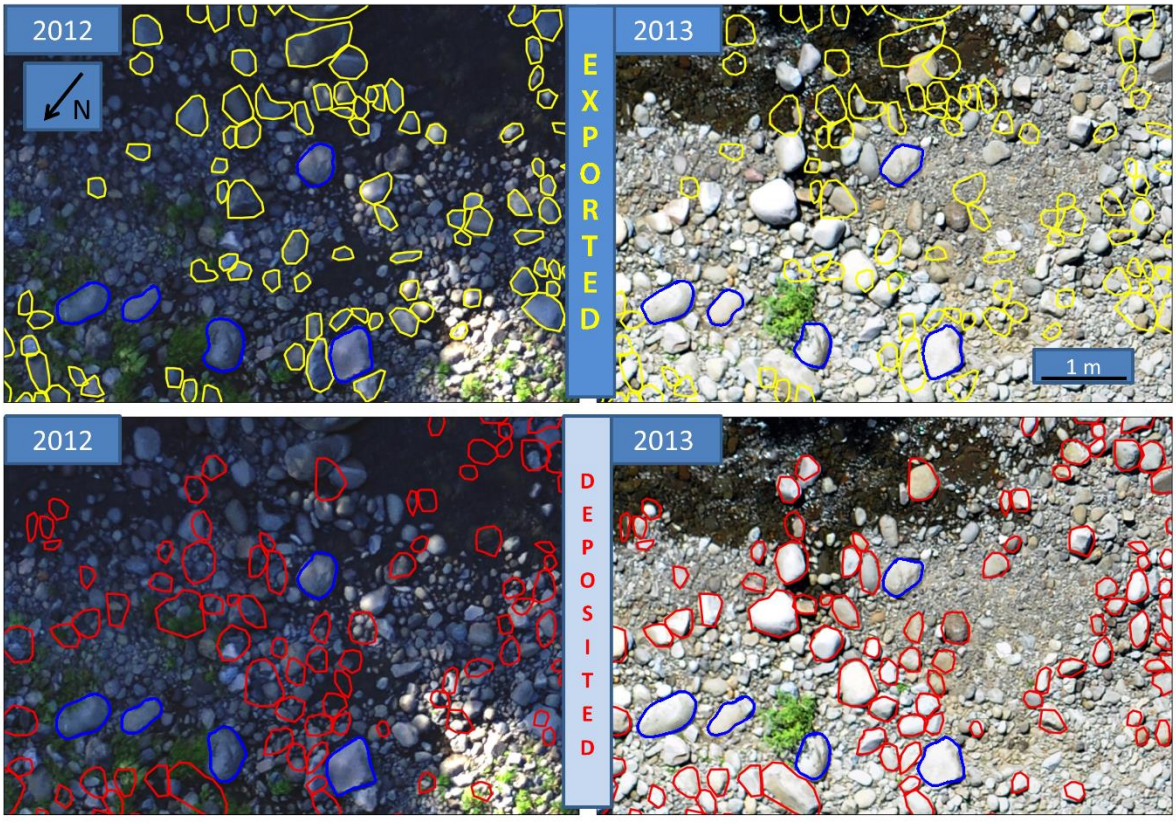

Figure 3: Example of surface change between 2012 (left) and 2013 (right). The upper pictures show the boulders that were exported between 2012 to 2013. The lower pictures show the boulders that were deposited during the same period. Some boulders, outlined in blue, visible in 2012 are still there in 2013. These static boulders belong to an indurated basal layer, or belong to the active layer and will be eventually exported.

https://doi.org/10.5194/esurf-2021-77
Preprint. Discussion started: 10 November 2021

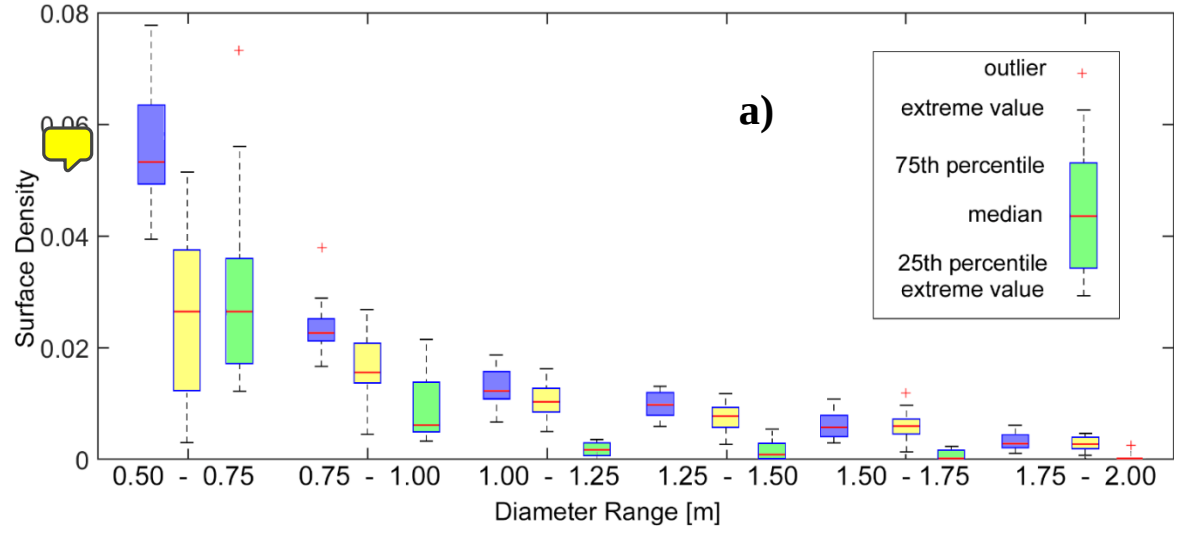

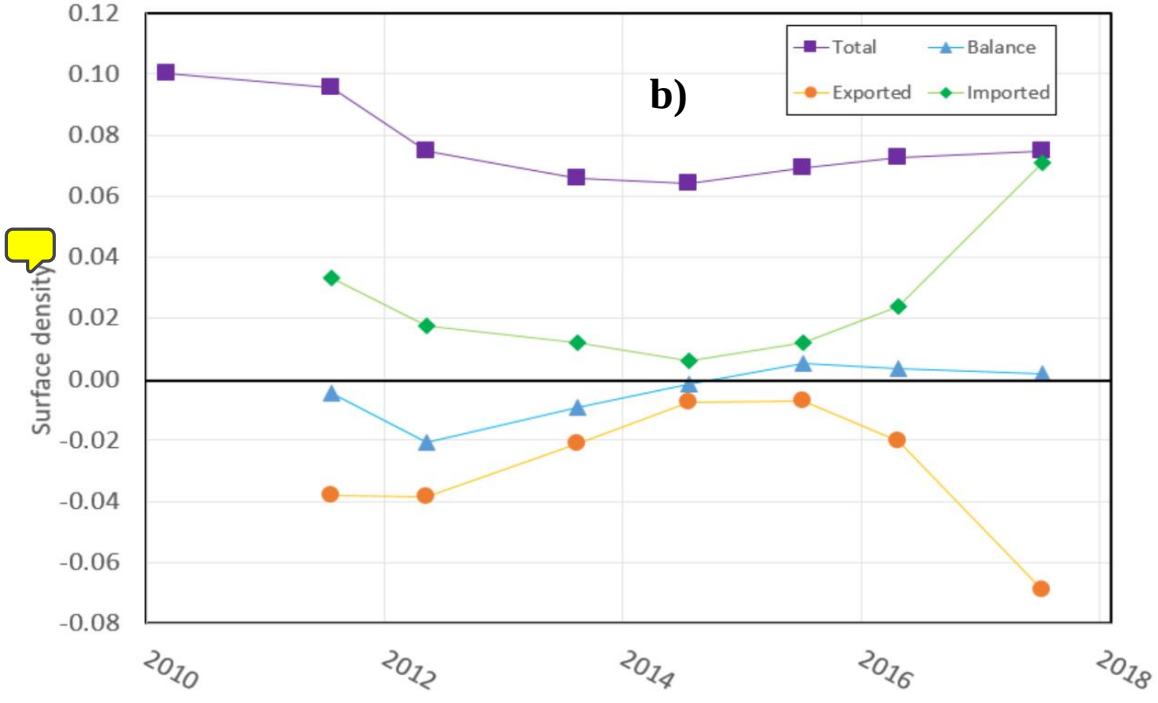

Figure 4: a) Box plot of the surface boulder density Eq. (1) on the bar as a function of the boulder diameter for the 8 years of our dataset. Blue: total number of boulders; green: freshly deposited boulders; yellow: boulders that were already in place during the preceding campaign of observation b) Surface density of exported, imported and total boulder population. The balance is almost at equilibrium, except from 2013 to 2014, during which years more sediment was exported than deposited. The cumulated surface of boulders decreased during 2012 and 2013. Data from 2010 have been obtain from a preliminary campaign.

https://doi.org/10.5194/esurf-2021-77
Preprint. Discussion started: 10 November 2021

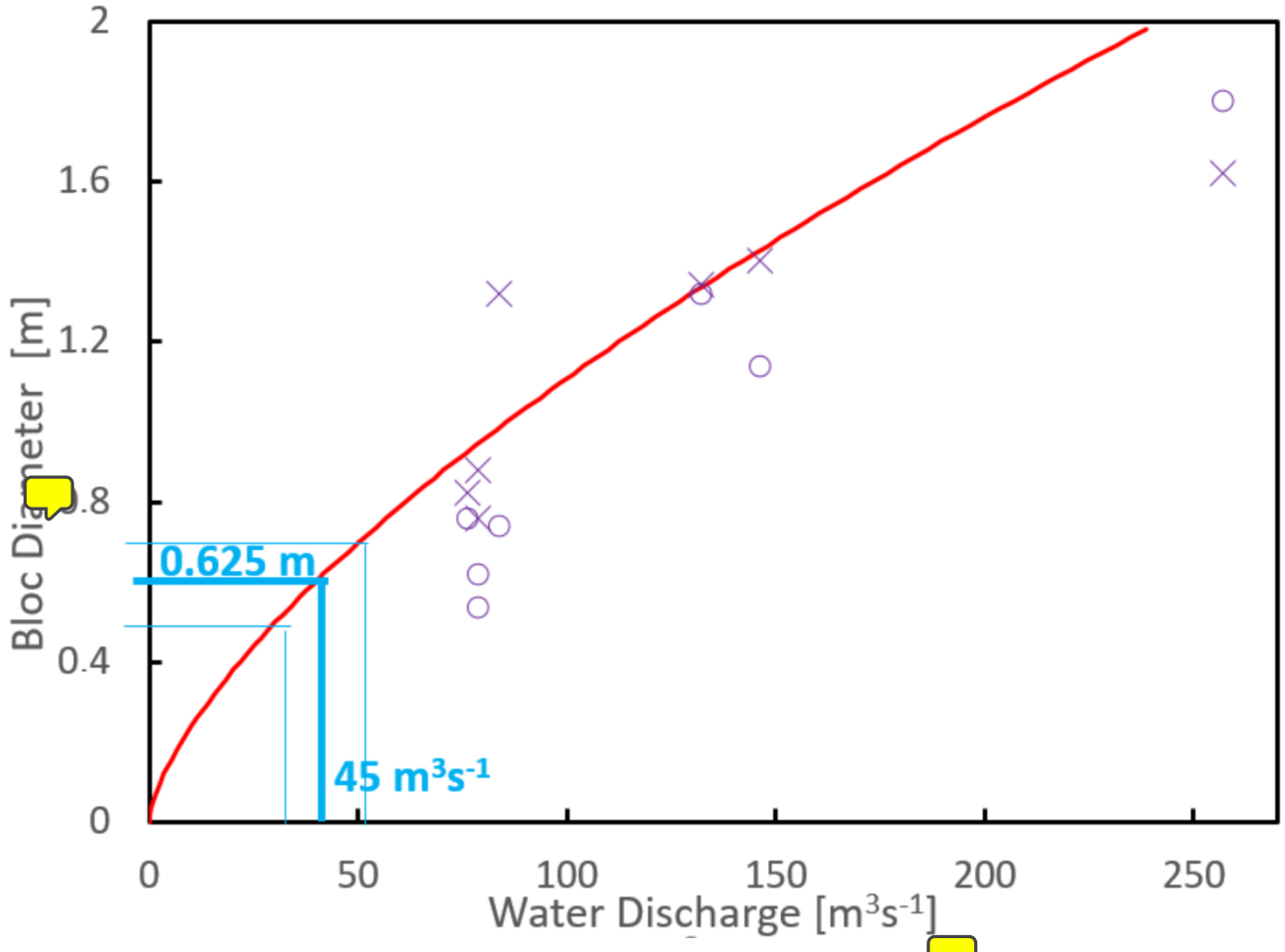

Figure 5: Maximum discharge recorded at the gauge station as a function of the size of the largest transported boulders from 2011 to 2018. The red curve represents the theoretical relation between water discharge and the maximum diameter of the exported or deposited boulders given by Eq. (2) (Appendix 1). The threshold discharge for boulders with a diameter of 0.625 m (center of D_1) can be estimated at about 45 $m^3\ s^{-1}$. The parameters used for the theoretical estimation of the flow threshold are: Darcy-Weisbach friction coefficient C_f=0.1, critical Shield number Θ_c= 0.02, width of river, W=30 m, $\Delta\rho$ the density difference between grains and water 1900 kg m^{-3}.

https://doi.org/10.5194/esurf-2021-77
Preprint. Discussion started: 10 November 2021

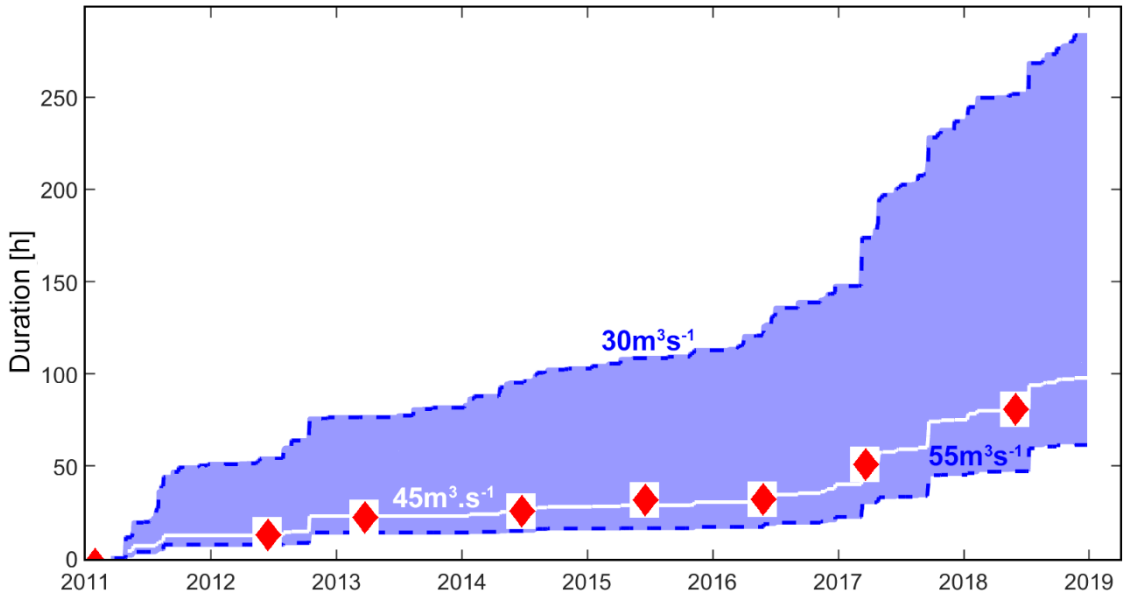

Figure 6: Cumulative duration of water discharge between 30 and 55 m^3s^{-1}. The white line represents a water discharge of 45 m^3s^{-1}. The transport is possible only a few hours each year, even during a hurricane year such as 2017. From 2014 to 2016, the transport time was less than 5 hours per year. The red diamonds indicate drone campaigns.

https://doi.org/10.5194/esurf-2021-77
Preprint. Discussion started: 10 November 2021

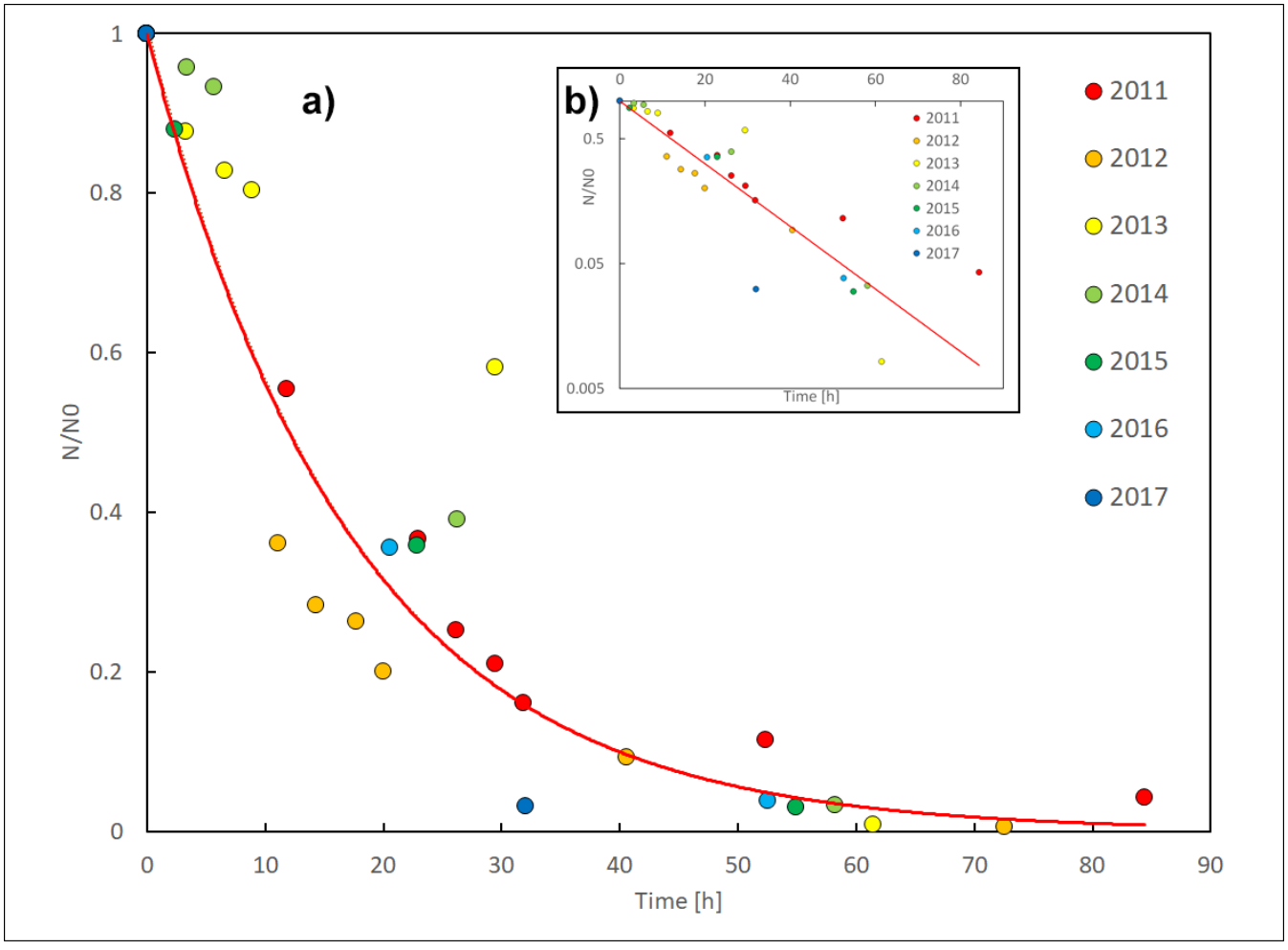

Figure 7: a) Evolution of the normalized number of boulders deposited on the bar between each campaign, and gradually entrained later. The horizontal axis is the transport time for a discharge threshold of 45 $m^3 h^{-1}$. The red curve is the best fit of Eq. 3 that is an exponential decay with a residence time of 17h (half-life of 12 h). That means that the boulders stay on average 17 hours on the bar and that half of the boulders are exported after 12 hours of transport time. B) The inset represents the same data in a semi-logarithmic scale.

https://doi.org/10.5194/esurf-2021-77
Preprint. Discussion started: 10 November 2021

Earth Surface Dynamics Discussions
Open Access
EGU

Diameter range [m]	0.50 - 0.75	0.75 - 1.00	1.00 - 1.25	1.25 - 1.50	1.50 - 1.75	1.75 - 2.00
Number of elements	438	93	30	17	10	3
Surface density [nb_grains	0.22660	0.04810	0.01550	0.00880	0.00520	0.00160
Mean grain volume [m^3]	0.06362	0.21471	0.44793	0.72464	1.20637	2.02014
Vol. Sed. discharge [$m^3\ h^{-1}$]	8	5	4	3	3	2
Threshold [$m^3.s^{-1}$]	45	70	100	135	176	220
Average annual duration of water disch. above threshold [h]	8	2.5	0.1875	0.125	0.05	0.01
Annual sed. disch [$m^3\ y^{-1}$]	61	14	0.7	0.4	0.2	0.02

Total Sed. discharge [$m^3.y^{-1}$]	**76**
Total sed discharge [$tons.y^{-1}$]	**220**

490 **Table 1: Bedload discharge estimates for boulders with D>0.5 m, assuming a residence time of 17h and a travel flight of 300 m. The total discharge is the sum over all bins. The total bedload discharge depends on the transport time averaged over the 8 years of study. We used Eq. (5) for these estimates.**